Available online at www.sciencedirect.com
SCIENCE DIRECT
Polymer 47 (2006) 5588–5595
polymer
www.elsevier.com/locate/polymer

Mesoscale modelling of penetrant diffusion in computer-generated polyethylene–spherulite-like structures

A. Mattozzi, P. Serralunga, M.S. Hedenqvist, U.W. Gedde *

School of Chemical Science and Engineering, Fibre and Polymer Technology, Royal Institute of Technology, SE-100 44 Stockholm, Sweden

Received 28 January 2005; received in revised form 10 May 2005; accepted 20 May 2005
Available online 26 May 2006

Abstract

Penetrant diffusion in semicrystalline polyethylene was simulated by first generating model spherulitic systems, and then, in the same systems, generating penetrant trajectories. Spherulitic growth was mimicked with an algorithm able to generate structures comparable to those observed in polyethylene. Current limitations in the number of lattice points of the system restricted the minimum amorphous layer thickness, which in turn limited the volume crystallinity range attainable to 0–35% and the crystal width-to-thickness ratio to ≤ 15. An on-lattice Monte–Carlo simulation assessed penetrant diffusion and the geometrical impedance factor was calculated and compared with the results obtained by the analytical method according to the Fricke theory. The combined effect of volume crystallinity and the crystal width-to-thickness ratio on the diffusivity was studied. A linear relationship was obtained between the geometrical impedance factor and the volume crystallinity at constant crystal width-to-thickness ratio, in accordance with the Fricke theory. The Fricke theory, however, underestimated the blocking effect of crystals of a given crystal width-to-thickness ratio, simply because it did not encounter the anisotropic lateral shape of the crystals and the continuous character of the branched lamellar crystals.

Keywords: Diffusion; Spherulite; Simulation

1. Introduction

The diffusion of small molecules in semicrystalline polymers is confined to the amorphous component, even though the smallest molecules (e.g. helium) can penetrate the polymer crystals [1]. The penetrant molecules are forced to circumvent the crystals and the lengthening of the diffusive trajectory is quantified by the geometrical impedance factor (τ)

$$\tau = \frac{D_a}{D \times \beta} \tag{1}$$

where D is the penetrant diffusivity in the semicrystalline material, D_a the penetrant diffusivity in the fully amorphous analogue and β the immobilization factor [2]. The factor β, which expresses the reduced segmental mobility of the constrained amorphous chain segments in the vicinity of a crystal surface, is conveniently described by free volume theory [3–11]. This paper addresses, however, only the purely geometric effect of the crystals expressed by the geometrical impedance factor, by comparing results obtained by simulation with those obtained by the Fricke theory. The immobilization factor was set to unity in all these calculations.

The structural dependence of the geometrical impedance factor of semicrystalline polymers has been predicted by empirical methods, i.e. curve fitting [2], theoretical arguments [2,11–16], and simulation [17,18], Analytical expressions have been derived to calculate the geometrical impedance factors in semicrystalline polymers by considering the crystallinity and the geometry of the crystals. These models assume that the polymer is composed of two components: impenetrable crystals and permeable amorphous material. Furthermore, they assume a simple, non-continuous geometry of the crystals. The Fricke theory [16], which was derived to explain the electrical conductivity in a two-component system of oblate spheroids in a continuous matrix, was later adapted by Michaels and Bixler [2] to apply to penetrant diffusion in a semicrystalline polymer

$$\tau = 1 + \frac{v_c\left[0.384 + \left(0.785 - \frac{L_c}{W}\right)^2\right]}{1.848 - 3\left(0.785 - \frac{L_c}{W}\right)^2} \tag{2}$$

* Corresponding author. Tel.: +46 8 7907640; fax: +46 8 208856.
E-mail address: gedde@polymer.kth.se (U.W. Gedde).

0032-3861/$ - see front matter © 2006 Elsevier Ltd. All rights reserved.
doi:10.1016/j.polymer.2005.05.162

where v_c is the volume crystallinity, L_c the crystal thickness and W the crystal width.

Simulation of diffusion has been widely used to predict permeation properties of polymers. Penetrant trajectories have been generated in fully amorphous polymers using molecular dynamics simulation [19–22]. Unfortunately, currently available molecular dynamics systems involve too a small material volume and ignore the multiphase character of the semicrystalline polymers, and thus give an inadequate description of the diffusion in these materials. Müller-Plathe [17] and Hadgett et al. [18] used a mesoscale approach to model the effect of crystallinity and crystal shape on the diffusivity. These studies were based on Monte–Carlo-generated random walks in both two- and three-dimensional lattices. Both studies considered the crystals as a group of non-percolating platelets embedded in an amorphous matrix. The results obtained by this simulation were essentially in accordance with the predictions made by the Fricke theory [18].

Hitherto reported mesoscopic simulations of the diffusion in semicrystalline polymers considered the crystals as isolated platelets, basically equiaxed in the fold surface plane. This is not a realistic model of the lamellar structure in polyethylene spherulites. It was realised many years ago that the number of crystal lamellae intersecting the growth boundary must be proportional to the square of the radial distance from the centre of the spherulite. This scale law is readily understood by simple arguments: (i) the crystallinity shows in most cases only a moderate variation within a single spherulite; and (ii) the dimensions of the crystals as viewed along the growth direction show only moderate variation within a single spherulite. These generalized facts imply that the number of crystals that intersect the growth boundary must be proportional to the boundary surface area, which in turn is proportional to the square of the radial distance from the spherulite centre. One solution to this problem is to picture the lamellar structure as continuous and highly branched, and to assume that the branches are at an angle with respect to the stem. David Bassett and associates at the University of Reading, UK were greatly involved in solving this problem using electron microscopy of permanganic etched samples; a method to reveal polyethylene crystals in melt-crystallized samples, which was developed by the Reading group [23,24]. They provided not only the missing morphological key element, branching with diverging crystal arms originating from a screw dislocation [25], but also the cause for the splaying, ciliation [26–28]. The extensive work of the Reading group, not only reporting the afore-mentioned findings, but also providing a wealth of additional information about the morphology of polyethylene, has been our inspiration and it has provided the information that has been used for spherulite building by simulation. A recent review of this and related topics has been written by two of the authors of this paper [29].

This paper presents the results of Monte–Carlo simulations generating penetrant trajectories in a spherulite-like morphology. The growth of the crystal nucleus into a spherulitic morphology using algorithms for lamellar branching and splaying generated the structure, which was the basis for the Monte–Carlo simulation of the penetrant diffusion. Morphological features, e.g. the spherulite radius, the crystal width-to-thickness ratio and the branching angle were systematically varied. Penetrant random walks simulated the diffusion, and the geometrical impedance factor was obtained by comparison with trajectories obtained in a fully amorphous model system. The results obtained by simulation were compared with the results obtained by the Fricke theory.

2. Theory and simulations

2.1. Spherulite growth by simulation

The simulations were performed using MATLAB 6 on a Macintosh Double 2 GHz Power PC G5 and a Pentium P3 processor PC. Even though care was taken to simulate the spherulite growth process as realistically as possible a few simplifications were still necessary. The growing crystal was assumed to have a rectangular lateral habit with a fixed width (W) and crystal thickness (L_c). The growth process was initiated from two opposite faces of a single crystal lamella. The crystal growth occurred in discrete steps by adding an infinitely stiff element, with the same width and thickness as the lamella nucleus and with a predefined length (gs). This element is displayed in Fig. 1 together with the definitions of the local coordinates used to control the growth process.

The element was defined by a set of numbers, the 'key point', that describe position (Fig. 1; point P), local coordinate system and growth direction. In addition, information concerning the activity status of the growing crystal lamella was recorded in the key point. Each key point was stored in a matrix ('kps') to enable retrieval of the complete growth history for further processing.

A cubic lattice was centred on the single initial lamella and the spherulite growth was prohibited outside a sphere inscribed in the cube, hence each cube contained one spherulite. The points of the cubic lattice were assigned the values one or zero, depending on whether they were located inside or outside the crystalline volume. The crystal thickness was always set to two lattice unit distances. The lattice unit distance is defined as the distance between two adjacent lattice points along the three orthogonal directions of the cubic lattice. The width of the crystal blocks was varied in the different simulations from 10 to 30 lattice unit distances. The values of the lattice points were stored in a 'box3D'matrix. This matrix could be scanned at high speed, e.g. for assessing the degree of crystallinity and its spatial distribution, or for penetrant diffusion purposes.

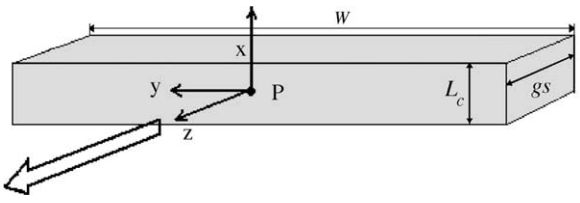

Fig. 1. The definition of the basic crystal element with a specified crystal thickness (L_c) and width (W). The arrow represents the direction of growth.

The local degree of crystallinity was assessed by defining cubes with 20 lattice unit edges and calculating the fraction of crystalline lattice units (fraction of lattice points with value 1) within that volume. The fully grown spherulite box thus contained 3375 of these small boxes used for local crystallinity assessment.

The growth of the crystal proceeded until it impinged on other crystals. Hence, the length of a crystal was not decided a priori. The crystal growth occurred basically free from cubic lattice. The placement of the lattice occurred in parallel with the growth of the crystals. An algorithm tested continuously that the space was free for adding a crystal block to the growing crystal. This algorithm was based on the cubic lattice, i.e. if any lattice point within the volume of the growth crystal block was occupied by another crystal (value = 1), the growth of the crystal was inhibited.

The branching process was described by five parameters. Fig. 2 shows the definition of the two vectors **u** and **v** that characterize the orientation of the branching crystal. Two angles identify the direction **u** of the lamellar branch: (a) the angle between the *z*-axis and the projection (**v**) of **u** on the **yz** plane, this angle being referred to as the splay angle; and (b) the angle between **v** and **u**, referred to as the split angle. The splay angle was varied between 20 and 40° and the split angle was varied between 15 and 30° in accordance with the morphological features characteristic of polyethylene reported by Bassett et al. [30–33]. The branching crystal also undergoes twisting about **u** (Fig. 2), which is parameterized by the length along the growth direction for making a 180° twist about **u**. The set of parameters was made in accordance with the morphological information provided by Patel and Bassett [34], the major part of the twist occurring near the lamellar branch region.

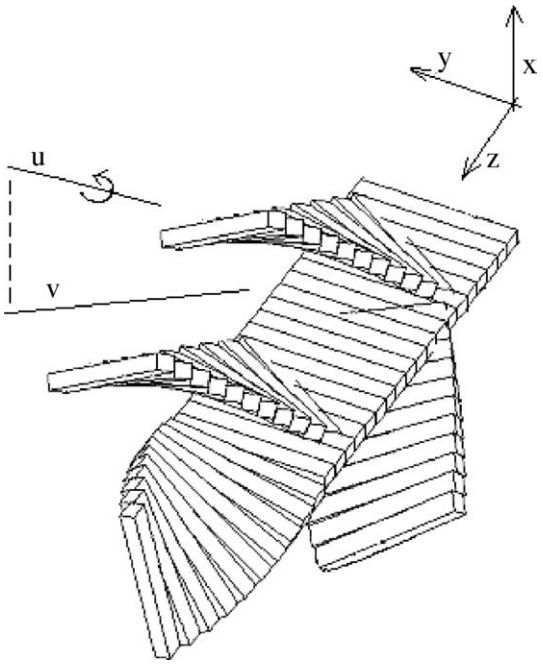

Fig. 2. Details of the lamellar branching. Vectors **z** and **u** are the growth directions of the initial and the branching lamella.

The frequency of lengthening (without branching or twisting), branching and twisting were set by the program by means of probability parameters, i.e. statistical weights; the sum of the three is equal to 1. The structure building by lengthening, branching or twisting was accomplished using random numbers.

The formation of the primary lamellae (branched, continuous structure originating from one crystal) constituted the first part of the growth process. The desired crystallinity was obtained by filling the remaining free space with 'new' secondary lamellae, which grew from the already existing primary lamellae (Fig. 3).

The morphological parameters that could be varied in the growth process were: crystal width, crystal thickness, branch and twist angles, minimum amorphous layer thickness and spherulite radius.

The secondary growth processes were needed to obtain a spherulite with uniform spatial distribution of crystals and the degree of crystallinity was evaluated continuously by considering the spherulitic growth to occur in steps through concentric shells. In most of the structures simulated six concentric shells were used. Each shell had a thickness of 25 lattice unit distances. The lamellae grew from one shell boundary to the next. If the crystallinity in a shell (control volume) was within acceptable limits ($\pm 10\%$ of the average volume crystallinity), the growth information in that shell was saved and the lamellae were allowed to continue to grow into the next shell. Otherwise, the growth in the shell was regenerated. A continuous spherulitic growth was ensured by

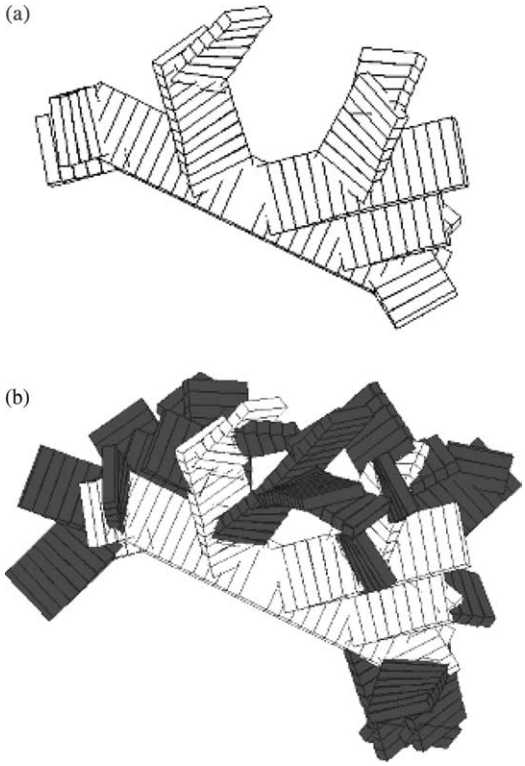

Fig. 3. (a) Initial stage of crystallisation with primary lamellae; (b) The formation of secondary lamellae (shown in darker colour).

restarting each shell-wise growth from the active ends of the existing lamellae in the previous shell.

2.2. Simulation of penetrant diffusion

The trajectory of a penetrant molecule was simulated with a lattice Monte–Carlo based random walk. The position of the penetrant was determined relative to a fixed reference frame (Lagrangian approach). The penetrant was allowed to move, with the same probability, to any of the nearest-neighbour sites. Each step was determined on the basis of a random number. The move was rejected if the lattice site was crystalline but the time step was still counted, as suggested by Müller-Plathe [17] and Hadgett et al. [18]. A continuous system of impinged spherulites was obtained by using spherical boundary conditions and wrapped coordinates. A penetrant molecule intersecting the spherulite boundary re-entered on the diametrically opposite position of the spherulite. The penetrant trajectory was obtained by unwrapping its coordinates.

2.3. Calculation of the penetrant diffusivity and the geometrical impedance factor

The penetrant diffusivity (D) was calculated from the Einstein equation [35]

$$D = \frac{\lim_{t\to\infty} \left\langle (\mathbf{r}(t) - \mathbf{r}(0))^2 \right\rangle}{6t} \tag{3}$$

where $\mathbf{r}$ is the displacement vector and t is time. The simulation had to be sufficiently long to ensure that any memory effects were absent and that the mean square-displacement versus t-curve was linear. In order to improve the statistics, each new penetrant position was considered as a start position for a new trajectory. The calculation of the penetrant diffusivity in each spherulite structure was based on 100 trajectories, each starting in a random-generated point and each consisting of 10^5 steps. The displacements are expressed in lattice units and the time scale is given as the number of performed diffusive steps.

The geometrical impedance factor (τ) of the spherulite-like structure thus built was determined according to Eqs. (1) and (2). The diffusivity data inserted in Eq. (1) was obtained by simulation using semicrystalline lattice (D) and a lattice without crystals (D_a). The factor β was set to unity in the calculations. The same structural parameters, volume crystallinity and crystal geometry (L_c and W), were inserted in Eq. (2) to calculate τ according to the Fricke theory.

3. Results and discussion

3.1. Spherulite structure

A fully grown spherulite is displayed in Fig. 4. The variation in the volume crystallinity in different regions of the spherulite is within the tolerances $\pm 10\%$ of the average volume crystallinity. The morphology was evaluated by analysing sections of the 'box3D' matrix. By using a grey-scale rather than a binary black and white, it was possible to mimic the variation in contrast that arises in electron micrographs of chlorosulphonated sections due to the fact that the crystals are oriented at different angles to the section surface. By summing the number of crystalline lattice points in the 'box3D'-matrix in the thickness direction for each xy coordinate and assigning a certain grey value to it, it was possible to obtain a two-dimensional grey scale-surface. Regions with a sharp black-to-white boundary indicated that the normal to the fold surface was parallel to the cut section surface. Fig. 5 shows a cross-section of a spherulite obtained in this way. The similarity between the simulated structure and the experimentally

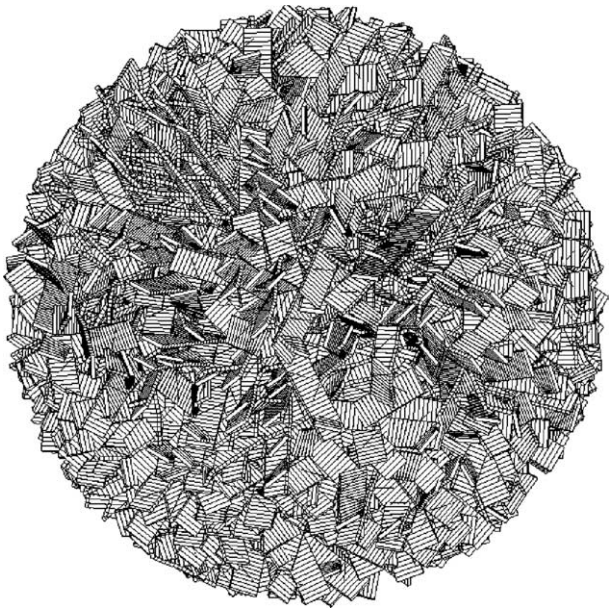

Fig. 4. A fully grown spherulite.

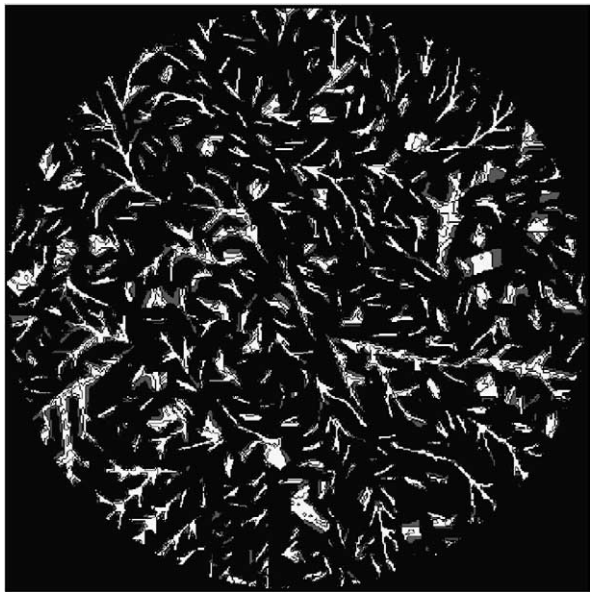

Fig. 5. Simulated electron micrograph of stained structure from a mature spherulite.

observed structure of polyethylene, in this case a permanganic-etched sample, is striking (Fig. 6(a) and (b)).

The crystal width-to-thickness ratio (W/L_c) ratio was varied between 5 and 15. The volume crystallinity was controlled by variation of the number of secondary growth stages, i.e. by setting the minimum amorphous layer thickness, the splitting and the splaying angles. The numerics—a lattice is placed 'on' the built spherulite structure with a maximum of 3×10^7 lattice points—sets the lower limit of the amorphous layer thickness to L_c. Hence, the maximum attainable volume crystallinity is 50%. In practice, however, the packing of the crystals never reached this crystallinity because of a lack of perfect orientation. Fig. 7 shows that a high splay angle was more effective than a high split angle in reducing the volume crystallinity. However, equally important was the W/L_c ratio, since the attainable volume crystallinity decreased with

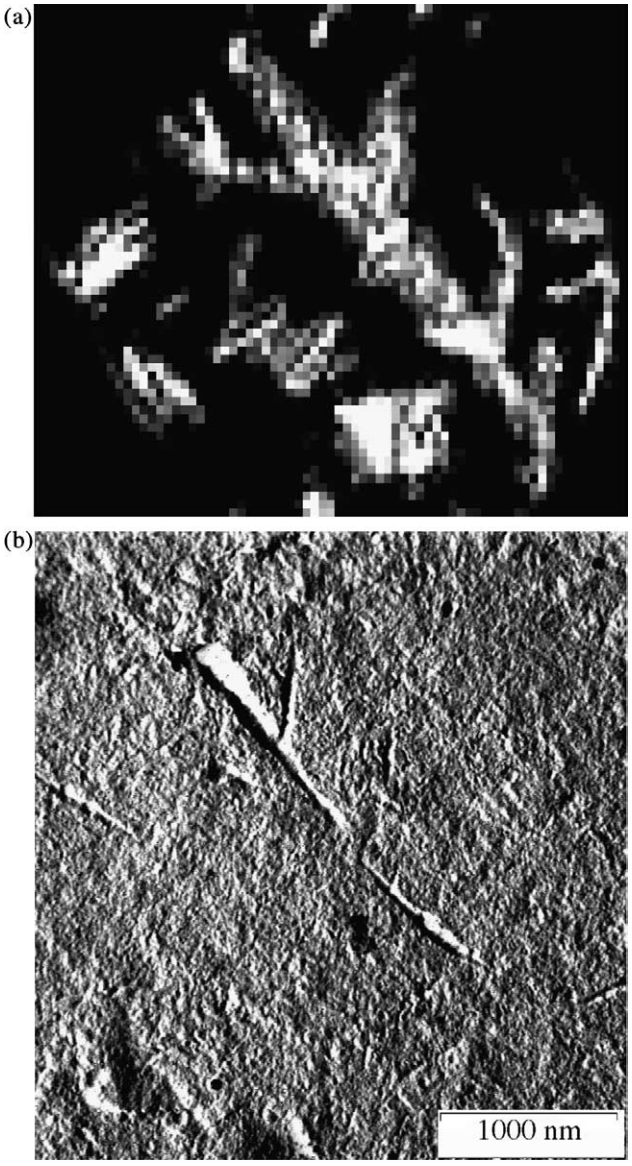

Fig. 6. Comparison between a simulated structure (a) and an electron micrograph of a replica of a permanganic-etched poly(ethylene-*co*-octene) (b).

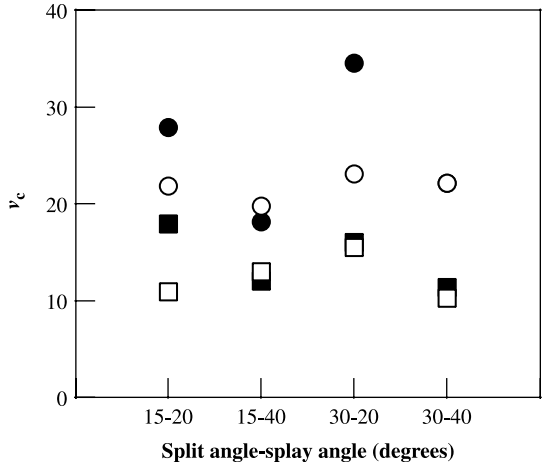

Fig. 7. The volume crystallinity as a function of the chosen split and splay angles for (●)W/L_c =5, (○)W/L_c =7.5, (■)W/L_c =10 and (□)W/L_c =15. The gs was 2 lattice units.

increasing W/L_c: $W/L_c=5$, $v_c=19$–35%; $W/L_c=7.5$, $v_c=20$–24%; $W/L_c=10$, $v_c=11$–18%; $W/L_c=15$, $v_c=10$–18%. The simulations performed with crystals with $W/L_c=15$ yielded spherulites with a considerable internal variation in crystallinity. Mattozzi et al. [9] reported for a series of homogeneous poly(ethylene-*co*-octene)s W/L_c values between 21 and 338. The samples with low crystallinity showed the highest values. The polymer with $W/L_c=21$ had a mass crystallinity of 78%. Hence, the built spherulites are not perfect copies of the real structure. The crystal ribbons have too low W/L_c values at a given volume crystallinity and spherulites with volume crystallinities greater than 35% cannot be generated. The structures built are therefore referred to as only spherulite-like.

Various actions would increase the crystallinity range attainable and would improve the structure building. The use of a finer lattice placed on the built structure would enable the setting of lower minimum amorphous layer thicknesses and thus higher crystallinities would be attained. The simulated crystals are infinitely stiff, and a modification to permit bending would provide a means to pack the crystals more efficiently. The constant width of the crystal ribbons may be relaxed; crystal growth along the *a*-axis must be possible and this would allow crystals with higher crystal width-to-thickness ratio to be used. The currently used starting structure with only one flat crystal block might also be changed.

3.2. Penetrant diffusivity

Fig. 8 shows the mean square displacement of a penetrant molecule versus time based on 100 random walks of 10^5 steps each in a spherulitic system with a cube side length of 301 lattice points together with the mean squares of the three orthogonal components of the displacement. Each random walk was started at a randomly chosen amorphous lattice point. The slope coefficient of the mean square displacement—time line was used to calculate the diffusivity according to Eq. (3).

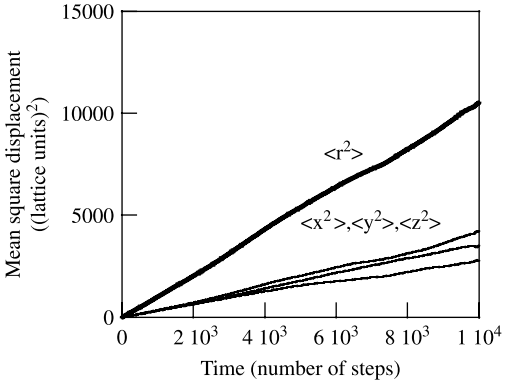

Fig. 8. Mean square displacement $\langle \mathbf{r}^2 \rangle$ in (lattice units)^2 as a function of time (in number of time steps) for a penetrant molecule doing 100 trajectories, each trajectory consisted of 10^5 steps (thick line). The displacements along the three Cartesian coordinate axes, $\langle \mathbf{x}^2 \rangle$, $\langle \mathbf{y}^2 \rangle$ and $\langle \mathbf{z}^2 \rangle$, sampled from the same trajectories are shown by the thin lines.

The goodness of the linear fit indicated the reliability of the calculated diffusivity. The mean square displacement curves along the three orthogonal directions were practically identical (Fig. 8). These data were averages based on 100 trajectories and the equality of the square displacements along the three orthogonal axes was expected. The individual penetrant trajectories showed a marked difference in the square displacements between the different orthogonal axes after an initial period (corresponding to ~100 jumps) of approximate equality between the three orthogonal square displacements (Fig. 9); the length scale of the diffusive process of 100 jumps is six lattice units, corresponding approximately to the size of the interlamellar distance. Hence, the motion within this threshold must be isotropic. On the times scales corresponding to from 100 to at least 300 jumps, matching length scales between 6 and 15 lattice units, hence in the size of lamellar width, the penetrant molecule motion was slower along at least

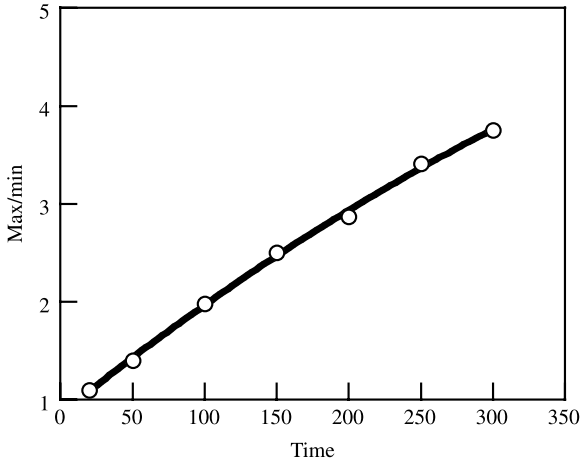

Fig. 9. The ratio between the maximum and the minimum square displacements (along **x**, **y** and **z**) for single penetrant molecule trajectory as a function of diffusive time (in number of time steps). System characteristics: volume crystallinity = 27.9%, crystal thickness = 2 lattice units. The standard deviations of the average data based on 30 trajectories were as follows: time = 50, 0.37; time = 100, 0.72; time = 150; 1.33; time = 200, 1.50; time = 250, 1.83; time = 300, 2.00.

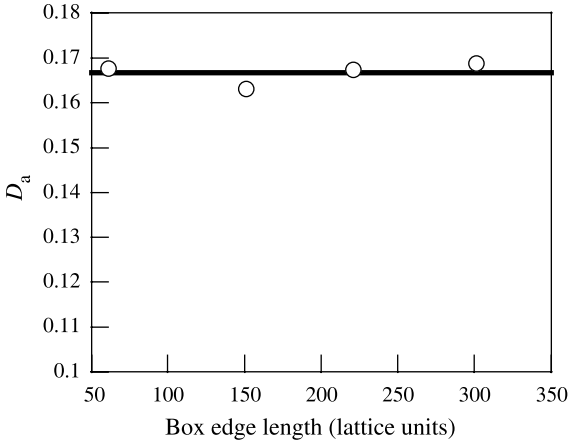

Fig. 10. Effect of box size on the diffusivity in a fully amorphous lattice. The continuous line shows the average of the diffusivity values obtained.

one axes. This anisotropic diffusion is believed to be due to the blocking effect of the crystals. It is believed that diffusion again becomes isotropic on even longer time/length scales.

Generating penetrant trajectories in a cube with only amorphous lattice points having different side lengths tested the effect of the spherical boundary condition on the diffusivity values obtained. The diffusivity was practically unaffected by a change in the size of the system, which indicated that the boundary conditions were adequate (Fig. 10). The average diffusivity was 0.167 with a RMS variation equal to 0.002 (1.5%).

3.3. Penetrant diffusivity as a function of volume crystallinity and crystal width-to-thickness ratio

Fig. 11 shows the geometrical impedance factor τ as a function of the volume crystallinity for a group of spherulitic structures with W/L_c adjusted to 5 and a cube side length equal to 301 lattice points. The analytical equation (Eq. (2))

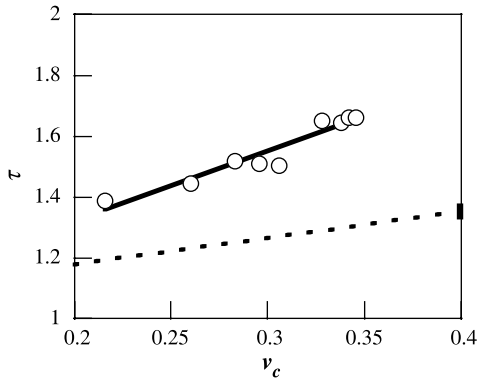

Fig. 11. The geometrical impedance factor as a function of volume crystallinity for a series of samples with $W/L_c = 5$ and cube side length equal to 301 lattice points. The continuous line was obtained by fitting Eq. (2) to the data obtained by simulation; the optimum value of the adjustable parameter (W/L_c) became 9.6. The dotted line shows the predicted values for the geometrical impedance factor for $W/L_c = 5$ according to Eq. (2). Parameter settings: splay angle = 20°; split angle = 30°; gs = 2 lattice units.

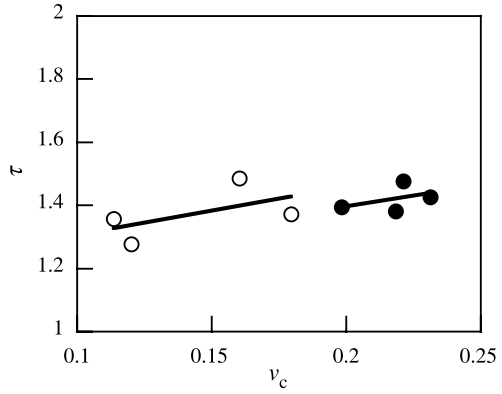

Fig. 12. The geometrical impedance factor as a function of volume crystallinity for systems with $W/L_c = 7.5$ (●; the line was obtained by fitting of Eq. (2); the optimum $W/L_c = 10$) and $W/L_c = 10$ (○; the line was obtained by fitting of Eq. (2); the optimum $W/L_c = 13$). The cube side length of structure included 301 lattice points; the gs was two lattice units.

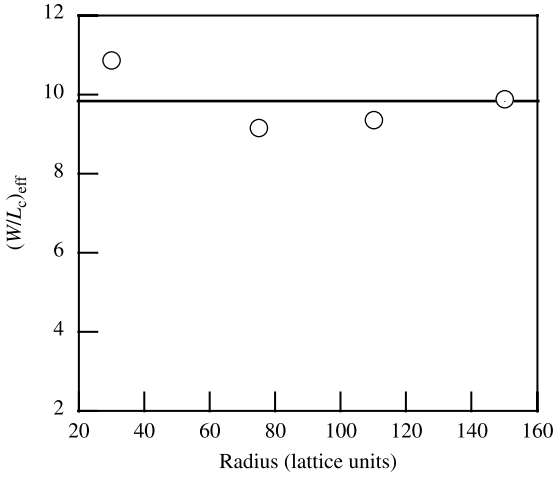

Fig. 13. Effect of spherulite radius on the penetrant diffusivity expressed in the effective W/L_c ratio. The crystal ribbons had a $W/L_c = 5$. The line shows the average of the data obtained.

and the simulations both yielded a linear relationship between the geometrical impedance factor and the volume crystallinity (Fig. 11). The τ data obtained by simulation were, however, significantly higher than the values predicted by the Fricke theory (with $W/L_c = 5$). By treating the W/L_c ratio as an adjustable parameter, it was possible to fit Eq. (2) to the τ data obtained by simulation; in this case, the ratio W/L_c became equal to 9.6. Obviously, the Fricke theory underestimated the geometrical impedance factor of the crystals by not considering that the crystals were significantly larger along the spherulite radial direction than in the perpendicular direction. The Fricke theory also underestimated the systems with W/L_c ratios of 7.5 and 10 (Fig. 12). The systems with W/L_c ratios of 15 showed a geometrical impedance factor lower than that predicted by the Fricke theory. This unexpected result was attributed to the presence a large and continuous pockets of amorphous material in the simulated structures.

The effect on the penetrant diffusivity of the structure variation along the spherulite radius was determined by dividing a built spherulite into four concentric spheres with different radii and calculating the diffusivity within each sphere. A spherulite that showed a low variation ($\pm 1\%$) in the crystallinity along the radius was used. Fig. 13 shows the effective W/L_c ratio of the structures according to the Fricke theory plotted as a function of the spherulite radius. The average effective W/L_c ratio was 9.8 and the RMS was 0.8 (7%). Hence, it is evident that the spherulite radius had only a negligible effect on the diffusivity. The establishment of a constant geometrical impedance factor already for the concentric shell with the smallest radius indicated that the 'extra' blocking effect due to the fact that the crystals were growing 'continuously' along the radial direction was established already at the early stage of spherulite growth.

4. Conclusions

An algorithm to generate spherulite-like arrangements of crystal lamellae was developed. Crystals were growing from a central nucleus in the spherulite radius direction. Crystal branching and splaying and secondary crystal nucleation yielded a uniform crystallinity along the spherulite radius. Current limitations in the number of lattice points of the system restricted the minimum amorphous layer thickness, which in turn limited the crystallinity range attainable to 0–35% and the crystal width-to-thickness ratio to ≤ 15. The penetrant trajectories performed by on-lattice Monte–Carlo simulation on the built spherulitic structure obeyed the Einstein equation even after short periods of diffusive time. The statistics obtained from single penetrant molecule trajectories indicated an anisotropic diffusive motion at intermediate times scales, which is believed to be due to blocking effect of the crystals. The crystallinity dependence of the geometrical impedance factor at a given crystal width-to-thickness ratio was linear, which is in accordance with the prediction made by the Fricke theory. However, the Fricke theory (for a given crystal width-to-thickness-ratio) underestimated the geometrical impedance factor, which can be explained by the continuity of the crystals from the centre of the spherulite to its periphery.

Acknowledgements

The financial support from the Swedish Research Council (grant 621-2001-1621) is gratefully acknowledged.

References

[1] Vieth WR. Diffusion in and through polymers. Hanser: Munich; 1991.
[2] Michaels AS, Bixler HJ. J Polym Sci 1961;5:413.
[3] Cohen MH, Turnbull D. J Chem Phys 1959;31:1164.
[4] Turnbull D, Cohen MH. J Chem Phys 1970;52:3038.
[5] Fujita H. Fortschr Hochpolym Forsch 1961;3:1.
[6] Hedenqvist M, Angelstok AA, Edsberg L, Larsson PT, Gedde UW. Polymer 1996;37:2887.
[7] Neway B, Hedenqvist MS, Gedde UW. Polymer 2003;44:4003.
[8] Neway B, Hedenqvist MS, Mathot VBF, Gedde UW. Polymer 2001;42:5307.
[9] Mattozzi A, Neway B, Hedenqvist MS, Gedde UW. Polymer 2005;46:929.
[10] Fels M, Huang RYM. J Appl Polym Sci 1970;14:523.

[11] Fleisher G. Colloid Polym Sci 1984;262:919.
[12] Michaels AS, Bixler HJ, Fein HL. J Appl Phys 1964;35:3165.
[13] Hedenqvist M, Gedde UW. Prog Polym Sci 1996;21:299.
[14] Boyd RH. J Polym Sci, Polym Phys Ed 1983;21:505.
[15] Michaels AS, Parker RB. J Polym Sci 1959;41:53.
[16] Fricke H. Phys Rev 1924;24:575.
[17] Muller-Plathe F. Chem Phys Lett 1991;177:527.
[18] Hadgett PM, Goldbeck-Wood G, Windle AH. Polymer 2000;41:6151.
[19] Müller-Plathe F, Rogers SC, Gunsteren WFv. Macromolecules 1992;25:6722.
[20] Hahn O, Mooney DA, Müller-Plathe F, Kremer K. J Chem Phys 1999;111:6061.
[21] Han J, Boyd RH. Polymer 1996;37:1797.
[22] Han J, Boyd RH. Macromolecules 1994;27:5365.
[23] Olley RH, Hodge AM, Bassett DC. J Polym Sci, Polym Phys 1979;17:627.
[24] Bassett DC, Hodge AM. Proc R Soc London 1978;A359:121.
[25] Bassett DC, Olley RH, Al Rehail IAM. Polymer 1988;29:1539.
[26] Teckoe J, Bassett DC. Polymer 2000;41:1953.
[27] Hosier IL, Bassett DC. Polymer 2000;41:8801.
[28] Hosier IL, Bassett DC. Polymer 2002;43:307.
[29] Gedde UW, Mattozzi A. Adv Polym Sci 2004;169:29.
[30] Bassett DC. CRC Crit Rev 1984;12:97.
[31] Bassett DC, Olley RH. Polymer 1984;(25):935.
[32] Bassett DC, Vaughan AS. Polymer 1985;26:717.
[33] Bassett DC, Hodge AM. Proc R Soc London 1981;A377:61.
[34] Patel D, Bassett DC. 2002;43:3795.
[35] Einstein A. Ann Phys 1905;17:549.